

This work was written as part of one of the author's official duties as an Employee of the United States Government and is therefore a work of the United States Government. In accordance with 17 U.S.C. 105, no copyright protection is available for such works under U.S. Law.

Public Domain Mark 1.0

<https://creativecommons.org/publicdomain/mark/1.0/>

Access to this work was provided by the University of Maryland, Baltimore County (UMBC) ScholarWorks@UMBC digital repository on the Maryland Shared Open Access (MD-SOAR) platform.

**Please provide feedback**

Please support the ScholarWorks@UMBC repository by emailing [scholarworks-group@umbc.edu](mailto:scholarworks-group@umbc.edu) and telling us what having access to this work means to you and why it's important to you. Thank you.

# Optical properties of boreal region biomass burning aerosols in central Alaska and seasonal variation of aerosol optical depth at an Arctic coastal site

T. F. Eck,<sup>1,2</sup> B. N. Holben,<sup>1</sup> J. S. Reid,<sup>3</sup> A. Sinyuk,<sup>1,4</sup> E. J. Hyer,<sup>3</sup> N. T. O'Neill,<sup>5</sup> G. E. Shaw,<sup>6</sup> J. R. Vande Castle,<sup>7</sup> F. S. Chapin,<sup>8</sup> O. Dubovik,<sup>9</sup> A. Smirnov,<sup>1,4</sup> E. Vermote,<sup>10</sup> J. S. Schafer,<sup>1,4</sup> D. Giles,<sup>1,4</sup> I. Slutsker,<sup>1,4</sup> M. Sorokine,<sup>1,4</sup> and W. W. Newcomb<sup>1,4</sup>

Received 29 July 2008; revised 10 February 2009; accepted 7 April 2009; published 2 June 2009.

[1] Long-term monitoring of aerosol optical properties at a boreal forest AERONET site in interior Alaska was performed from 1994 through 2008 (excluding winter). Large interannual variability was observed, with some years showing near background aerosol optical depth (AOD) levels ( $<0.1$  at 500 nm) while 2004 and 2005 had August monthly means similar in magnitude to peak months at major tropical biomass burning regions. Single scattering albedo ( $\omega_0$ ; 440 nm) at the boreal forest site ranged from  $\sim 0.91$  to 0.99 with an average of  $\sim 0.96$  for observations in 2004 and 2005. This suggests a significant amount of smoldering combustion of woody fuels and peat/soil layers that would result in relatively low black carbon mass fractions for smoke particles. The fine mode particle volume median radius during the heavy burning years was quite large, averaging  $\sim 0.17 \mu\text{m}$  at AOD(440 nm) = 0.1 and increasing to  $\sim 0.25 \mu\text{m}$  at AOD(440 nm) = 3.0. This large particle size for biomass burning aerosols results in a greater relative scattering component of extinction and, therefore, also contributes to higher  $\omega_0$ . Additionally, monitoring at an Arctic Ocean coastal site (Barrow, Alaska) suggested transport of smoke to the Arctic in summer resulting in individual events with much higher AOD than that occurring during typical spring Arctic haze. However, the springtime mean AOD(500 nm) is higher during late March through late May ( $\sim 0.150$ ) than during summer months ( $\sim 0.085$ ) at Barrow partly due to very few days with low background AOD levels in spring compared with many days with clean background conditions in summer.

**Citation:** Eck, T. F., et al. (2009), Optical properties of boreal region biomass burning aerosols in central Alaska and seasonal variation of aerosol optical depth at an Arctic coastal site, *J. Geophys. Res.*, 114, D11201, doi:10.1029/2008JD010870.

## 1. Introduction

[2] Boreal forests are one of the largest biomes on earth, comprising  $\sim 14.5\%$  of the Earth's land surface or  $\sim 16$  million square kilometers across northern Eurasia and North America. The arctic and boreal zones currently store the globe's largest reservoir of soil carbon, at 25–35% of the total, largely in organic soil layers in the permafrost [Bonan and Shugart, 1989; Melillo et al., 1995]. Both climate change simulations of the effects of increasing atmospheric greenhouse gas concentrations and recent observations show that global temperature increases are the largest in the arctic and

boreal regions [Soja et al., 2007; Intergovernmental Panel on Climate Change (IPCC), 2007]. As a result of these temperature increases (and drier conditions) models predict future increases in area burned in the boreal zone. For example, Flannigan et al. [2005] simulated a 74–118% increase in burned area in Canada by 2100 in a 3XCO<sub>2</sub> increase scenario. Kharuk et al. [2008] found a one-third reduction in fire return interval time for larch dominated forests in Siberia from the 19th to the 20th century, related to warming temperatures in northeast Siberia. Severe forest fires that also burn insulating organic and peat soil layers result in deeper soil thawing [Kharuk et al., 2008] and thereby may release large amounts of stored carbon into the atmosphere.

<sup>1</sup>Biospheric Sciences Branch, NASA, GSFC, Greenbelt, Maryland, USA.

<sup>2</sup>Goddard Earth Sciences and Technology Center, University of Maryland, Baltimore, Maryland, USA.

<sup>3</sup>Aerosol and Radiation Section, Naval Research Laboratory, Monterey, California, USA.

<sup>4</sup>Science Systems and Applications, Inc., Lanham, Maryland, USA.

<sup>5</sup>CARTEL, Université de Sherbrooke, Sherbrooke, Quebec, Canada.

<sup>6</sup>Geophysical Institute, University of Alaska, Fairbanks, Alaska, USA.

<sup>7</sup>Biology Department, University of New Mexico, Albuquerque, New Mexico, USA.

<sup>8</sup>Institute of Arctic Biology, University of Alaska, Fairbanks, Alaska, USA.

<sup>9</sup>Laboratoire d'Optique Atmosphérique, CNRS Université de Lille, Villeneuve d'Ascq, France.

<sup>10</sup>Department of Geography, University of Maryland, College Park, Maryland, USA.

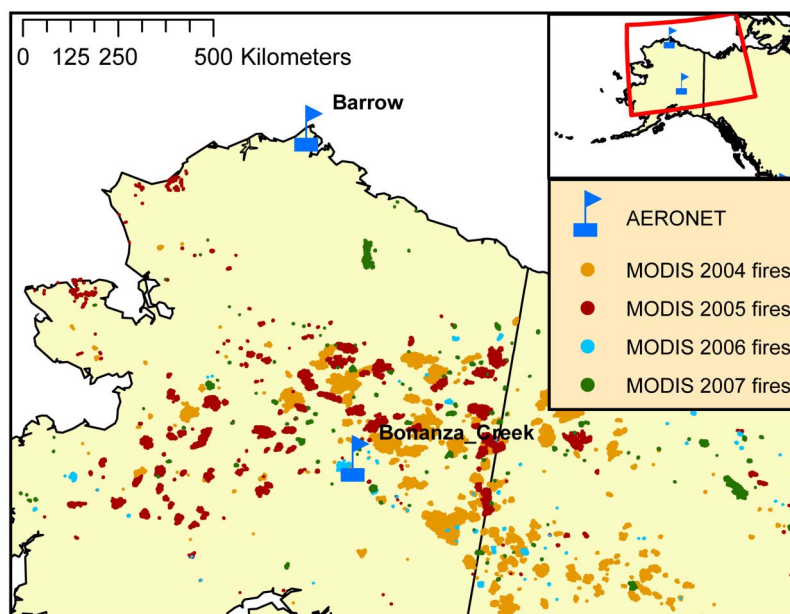


**Figure 1.** Map of Alaska showing the AERONET sites at Bonanza Creek in the central boreal forest zone and Barrow on the arctic coast of the Beaufort Sea. Also shown are the fires detected by the MODIS sensor on the Terra satellite for the years 2004 through 2007.

[3] Concurrent with a significant warming trend, *Kasischke and Turetsky* [2006] found that the annual boreal forest area burned in Alaska and Canada doubled from the 1960s/1970s to the 1980s/1990s and the proportion of burning in the early and late growing seasons increased. In Alaska seven of the eleven largest fires in a 56 year interval (1950–2005) have burned since 1988, with the largest area burned on record occurring in 2004 and the third largest in 2005 [*Soja et al.*, 2007]. Across the entire circumboreal zone the frequency of extreme fire years has increased. *Kasischke et al.* [2002] have found that high fire years in Alaska consist of larger fires occurring later in the growing season. In low precipitation years peat burning is expected to increase as the summer advances due to deeper drying of the soil column. For the 2004 boreal fires in Alaska and Canada, *Turquetty et al.* [2007] estimated that ~37% of the carbon monoxide emissions resulted from peat burning and that ~17% of the total area burned was peat (assumed to burn exclusively in the smoldering phase). Currently boreal peatlands are a net sink of carbon from the atmosphere, however *Turetsky et al.* [2002] estimate that an increase of 17% in area and intensity of peatland burned annually would convert boreal peatlands to a net carbon source.

[4] Biomass burning aerosols generated from boreal zone burning may have significant impacts on regional direct radiative forcing and also may be transported deep into Arctic regions. The aerosol direct radiative effects are enhanced at polar latitudes due to long day length, large path length transmission through the aerosol layers and high underlying surface albedo of ice and snow. From modeled trajectory analyses, *Stohl* [2006] estimates that in the summer, during years of average burning, boreal fires contribute more aerosol black carbon (BC) to the Arctic than do anthropogenic sources. Extensive boreal fires in Russia (Lake Baikal region) in 2003, contributed an estimated ~50% of the BC deposited north of 75°N in spring

and summer of that year [*Generoso et al.*, 2007]. In addition to atmospheric radiative effects, the deposition of these aerosols onto snow and ice surfaces in the Arctic may reduce the albedo and lead to increased melting rates [*Hansen and Nazarenko*, 2004]. From Greenland ice cores *McConnell et al.* [2007] show large interannual variability in BC deposited by boreal fires over a 200-year interval, with BC from industrial sources dominating from 1890 to 1950. However, *Flanner et al.* [2007] have estimated from simulations that aerosol BC has maximum forcing potential on snow/ice albedo in April through June (earlier than many major boreal fires). Even in strong boreal burning years they attribute ~80% of the global BC/snow forcing to be from anthropogenic fossil fuel and biofuel sources.

[5] Only recently have studies investigated the optical properties of boreal region biomass burning aerosols in intensive burning years [*Stohl et al.*, 2006; *Myhre et al.*, 2007]. *Pfister et al.* [2008] discuss the need for better characterization of the optical properties of boreal region biomass burning smoke particles, especially for the case of significant peat burning. In this investigation we present an analysis of a long time series of aerosol optical depth measurements from 1994 through 2008 at an AERONET sun-sky radiometer site located in the boreal forest zone of central Alaska. In the extreme burning years of 2004 and 2005 the AOD was very high, allowing for accurate characterization of the spectral imaginary refractive index (absorption) and single scattering albedo ( $\omega_0$ ) from almucantar retrievals. Additionally, we compare the particle size distributions and  $\omega_0$  of these fine mode dominated smoke aerosols to the size distributions and absorption of smoke aerosols from other major biomass burning regions. We also present AOD data from a site on the Arctic Ocean coast in Alaska to compare the seasonality and frequency of smoke transport to the Arctic (primarily in summer) to the springtime Arctic haze impacts on optical depth. The Arctic haze phenomenon

has been attributed primarily to the long-distance transport of aerosols from industrial source regions [Shaw, 1995].

## 2. Instrumentation, Study Sites, and Techniques

### 2.1. Study Region and Sites

[6] The principal AERONET site analyzed in this study is the Bonanza Creek, Alaska site located in the boreal forest biome of central Alaska (Figure 1). This is a National Science Foundation Long-Term Ecological Research (LTER) Network site ~20 km west of Fairbanks (64°45'N, 148°32'W; elevation ~353 m), one of 26 network sites representing diverse ecosystems and research (<http://www.lternet.edu/sites/bnz/>). The data set at Bonanza Creek is one of the longest and most complete sets of aerosol optical properties measurements made at any site in the AERONET network, beginning in June 1994 and continuing through 2008, however missing 2001 and 2003 due to instrument and/or satellite transmitter problems. Due to the severely cold winter weather and deep snow, which makes operation of the sun-sky radiometer problematic and site access limited for maintenance, the CIMEL sun-sky radiometer is typically operated from April or May through October of most years (usually for ~5–7 months). Additionally AERONET AOD data from the Barrow, Alaska site (71°20'N, 156°40'W; elevation ~8 m) on the Arctic coast of the Beaufort Sea are analyzed to investigate the seasonality of column integrated aerosol concentrations from April through September. Similar to Bonanza Creek, data are not acquired in the other months due to both severely cold conditions and lack of sunlight for measurements. Both of these sites are located far from significant local sources of aerosol pollution such as industry and urbanization.

### 2.2. AERONET Instrumentation

[7] The CIMEL Electronique CE-318 sun-sky radiometer measurements reported in this paper were made with instruments that are a part of the AErosol RObotic NETwork (AERONET) global network. These instruments are described in detail in Holben *et al.* [1998], however a brief description will be given here. The automatic tracking Sun and sky scanning radiometers made direct Sun measurements with a 1.2° full field of view every 15 minutes at 340, 380, 440, 500, 675, 870, 940, and 1020 nm (nominal wavelengths). The direct sun measurements take ~8 seconds to scan all 8 wavelengths, with a motor driven filter wheel positioning each filter in front of the detector. These solar extinction measurements are then used to compute aerosol optical depth (AOD,  $\tau_a$ ) at each wavelength except for the 940 nm channel, which is used to retrieve total columnar (or precipitable) water vapor in centimeters. The filters utilized in these instruments were ion assisted deposition interference filters with bandpass (full width at half maximum) of 10 nm, except for the 340 and 380 nm channels at 2 nm. The estimated uncertainty in computed  $\tau_a$ , due primarily to calibration uncertainty, is ~0.010–0.021 for field instruments (which is spectrally dependent with the higher errors in the UV [Eck *et al.*, 1999]). Schmid *et al.* [1999] compared  $\tau_a$  values derived from four different solar radiometers (including an AERONET sun-sky radiometer) operating simultaneously together in a field experiment and found that the  $\tau_a$  values from 380 to 1020 nm agreed to within 0.015

(RMS), which is similar to our estimated level of uncertainty in  $\tau_a$  retrieval for field instruments. The spectral aerosol optical depth data have been screened for clouds following the methodology of Smirnov *et al.* [2000], which relies on the greater temporal variance of cloud optical depth versus aerosol optical depth. The sky radiances measured by the sun/sky radiometers are calibrated versus the 2-meter integrating sphere at the NASA Goddard Space Flight Center, to an absolute accuracy of ~5% or better.

### 2.3. Inversion Methodology

[8] The CIMEL sky radiance measurements in the almucantar geometry (fixed elevation angle equal to solar elevation and a full 360° azimuthal sweep) at 440, 675, 870, and 1020 nm (nominal wavelengths) in conjunction with the direct sun measured  $\tau_a$  at these same wavelengths were used to retrieve optical equivalent aerosol size distributions and refractive indices. Using this microphysical information the spectral dependence of single scattering albedo ( $\omega_s$ ) is calculated. The algorithm of Dubovik and King [2000] with enhancements detailed by Dubovik *et al.* [2006] was utilized in these retrievals, known as Version 2 AERONET retrievals. Level 2 quality assured retrievals [Holben *et al.*, 2006] are presented in this paper. The Version 2 AERONET algorithm determines the percentage of spherical particles required to give the best fit to the measured spectral sky radiance angular distribution. Further details on the Version 2 algorithm and the improved specification of surface bidirectional reflectance can be found in Dubovik *et al.* [2006] and Eck *et al.* [2008].

[9] Almucantar sky radiance measurements were made at optical air masses of 4, 3, 2, and 1.7 in the morning and afternoon, and once per hour in between. In order to ensure sky radiance data over a wide range of scattering angles, only almucantar scans at solar zenith angles greater than 50° are analyzed and presented here. To eliminate cloud contamination from the almucantar directional sky radiance data we require the radiances to be symmetrical on both sides of the sun at equal scattering angles. The stable performance of the inversion algorithm was illustrated in sensitivity studies performed by Dubovik *et al.* [2000] where the perturbations of the inversion resulting from random errors, possible instrument offsets and known uncertainties in the atmospheric radiation model were analyzed. Their work employed retrieval tests using known size distributions to demonstrate successful retrievals of mode radii and the relative magnitude of modes for various types of bimodal size distributions such as those dominated by a submicron accumulation mode or distributions dominated by supermicron coarse mode aerosols. To ensure sufficient sensitivity to aerosol absorption, only almucantar scans where AOD(440 nm) > 0.4 [Dubovik *et al.*, 2000] were analyzed for the investigation of the characteristics of spectral refractive indices and single scattering albedo.

## 3. Results and Discussion

### 3.1. Temporal and Spectral Variability of AOD in Central Alaska

#### 3.1.1. Monthly and Interannual Variation in AOD and Angstrom Exponent

[10] The monthly climatology of 500 nm AOD and Angstrom Exponent (440–870 nm) at Bonanza Creek,

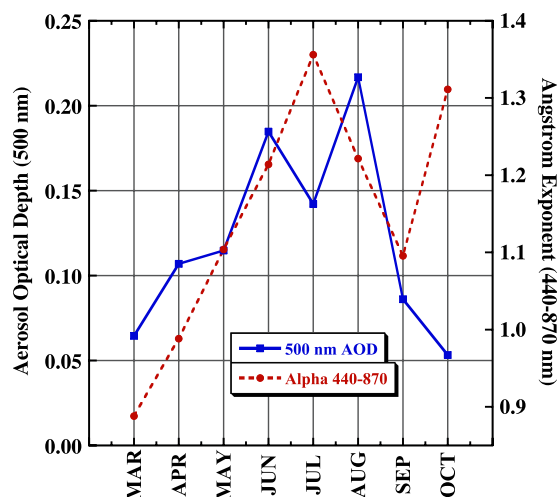


**Figure 2.** Multiyear monthly averages of aerosol optical depth at 500 nm and Angstrom exponent (440–870 nm) at Bonanza Creek for the time period 1994–2008.

Alaska showing monthly means from multiple years of observations is shown in Figure 2. The 440–870 nm Angstrom is computed from linear regression of  $\ln$  AOD versus  $\ln \lambda$  scale at 440, 500, 675 and 870 nm. The multiyear monthly means are computed as a mean of the individual monthly averages. The seasonal trend in monthly average AOD shows a steady increase of AOD from near background levels in March ( $\sim 0.06$ ) to values exceeding  $\sim 0.14$  for June, July and August and then a rapid 2-month decline down to background again ( $\sim 0.05$ ) in October. It should be noted that the interannual variability in AOD is extremely large (see Figure 3, discussed below) due to the episodic nature of boreal fires with severe and numerous fires occurring in drought years, compared to few fires in wet years. Fine mode biomass burning aerosols dominate this seasonality as the Angstrom exponent increases in summer (June–August) when most burning occurs.

[11] The year-to-year time series of monthly average AOD at 500 nm by year for the summer and early fall months (June–September) at Bonanza Creek is shown in Figure 3a. Monthly means are computed as an average of all daily means. Different numbers of daily means are averaged for each month due primarily to differing cloud cover that showed large interannual variability and month-to-month variability. The number of days averaged for each monthly mean varied from 4 to 29, with the maximum occurring in August 2004 when drought conditions prevailed. Variability within a month is often very high, for example, in June 2004 the mean AOD at 500 nm was 0.39 while the standard deviation was 0.86 (see also Figure 6 and related text). From 1994 until 2002 the only months with average AOD equal or exceeding 0.20 were July of both 1999 and 2000. Then in 2004 all four months showed monthly means exceeding 0.35 and in 2005 the AOD exceeded 0.20 in all months except September, which had a very low background level of 0.04 (typical of most Septembers but an order of magnitude less than September 2004). Particularly notable is the extremely high AOD in August of 2004 and 2005, both severe burning years. These monthly average AOD (500 nm) values of 0.98 and 0.70 for 2004 and 2005,

respectively, are of similar magnitude to monthly means of peak burning season months in major tropical biomass burning regions such as Zambia and southern Amazonia [Eck et al., 2003b; Schafer et al., 2008].

[12] The Terra satellite MODIS image from August 14, 2005 shows extensive smoke covering central Alaska with thick smoke plumes advecting from satellite identified hot spot fires (Figure 4 [Justice et al., 2002]). Remotely sensed fire counts for the Alaska region from the MODIS Terra satellite (Figure 5) also show a monthly total maximum in August 2004 and 2005, with counts much higher than during 2002, 2003, 2006, 2007, and 2008. However, in 2004 there were similar number of fires in July as August while the AOD at Bonanza Creek was  $>2.5$  times higher in August. Daily area burned estimates for Alaska and Canada combined as shown by Stohl et al. [2006] reach a maximum from late June through July, and much less area burned in August. This suggests the possibility that factors other than area burned and numbers of fires are important in determining the total atmospheric column AOD. Other factors in addition to area burned that would influence the AOD are meteorological conditions (including wind speed and direction, atmospheric stability, and precipitation), intensity of

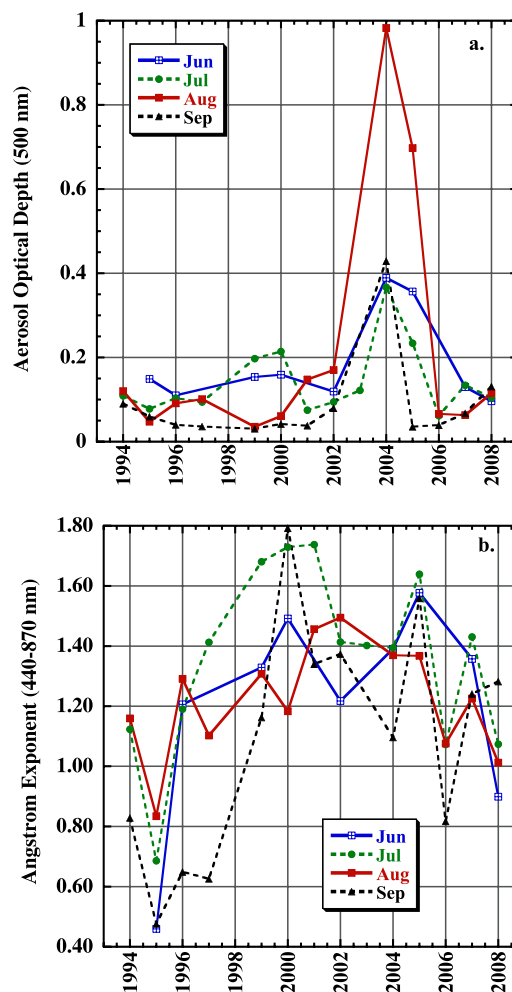


**Figure 3.** Time series of (a) monthly average AOD at 500 nm and (b) Angstrom exponent (440–870 nm) by year for the summer and early fall months (June–September) at Bonanza Creek.

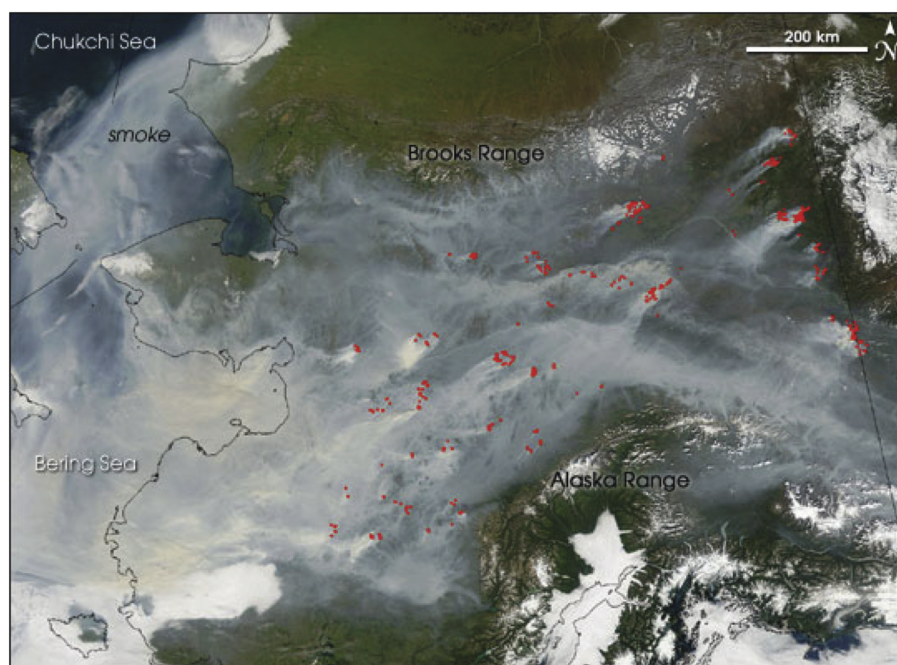


**Figure 4.** Terra MODIS image from 14 August 2005 showing extensive smoke covering central Alaska with thick smoke plumes advecting from satellite identified hot spot fires. Note that the smoke over land is largely confined south of the Brooks mountain range in the north and the Alaska Range in the south, while northward transport occurs to the east over the Chukchi Sea.

burning since intense fires enhance convection that may loft smoke to higher altitudes where winds are higher, and the types of fuel burned and the phase of combustion [Reid *et al.*, 2005b]. It is noted that AOD measurements at a point location (Bonanza Creek) are also strongly affected by the location of the fires in the entire state of Alaska relative to the wind direction and other meteorological factors. Satellite hot spot remote sensing robustly detects fires in the high temperature flaming phase of combustion but it is much more difficult to detect lower temperature smoldering phase fires. However, the flaming phase is typically of relatively short duration, while the larger diameter woody fuels in a forest and the organic soils and peatlands may burn for several days in the smoldering phase. As previously mentioned, Turquet *et al.* [2007] estimated that the proportion of carbon monoxide emissions was double the proportion of peat area burned ( $\sim 37\%$  of the carbon monoxide emissions from only 17% of the area burned) in 2004 for fires in Alaska and Canada. This suggests that peat burning may possibly also have resulted in a disproportionate amount of total aerosol emissions, relative to the total area burned.

[13] The Angstrom exponent computed over the spectral interval of 440 to 870 nm is a relative measure of the fine versus coarse mode contribution to the total AOD [Reid *et al.*, 1999; Eck *et al.*, 2001]. In Figure 3b we show the monthly mean time series of  $\alpha_{440-870}$  at Bonanza Creek, Alaska for the same data as shown in Figure 3a for the AOD. Variability within a month is not as high for  $\alpha_{440-870}$  as for AOD, with the coefficient of variation (standard deviation/mean  $\times 100$ ) typically about 20–40%, while for AOD it sometimes exceeds 100%. For most months in most years the Angstrom Exponent exceeds 1, thus indicating the dominance of fine mode sized particles [Eck *et al.*, 2005], which most likely originate from biomass burning. The year

1995 is the exception where all months have average  $\alpha_{440-870} \leq 0.9$ . This year has low monthly mean AOD in most months ( $<0.1$ , except June 1995 at  $\sim 0.15$ ), therefore a low near background level of coarse mode aerosols from various sources such as long distance transported Asian dust or sea salt, or even some thin cirrus contamination can have a very large effect on the reduction of  $\alpha_{440-870}$ . Additionally during months with low AOD the uncertainty in AOD of  $\sim 0.01$  results in very large uncertainty in Angstrom exponent. The monthly means of  $\alpha_{440-870}$  for September (all years) show the widest range, from  $<0.5$  to 1.8, due partly to

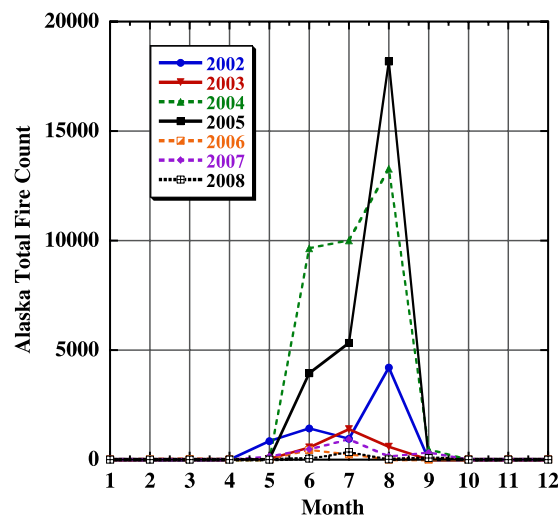


**Figure 5.** Remotely sensed fire counts for the Alaska region from the MODIS sensor on the Terra satellite for the years 2002 through 2008.

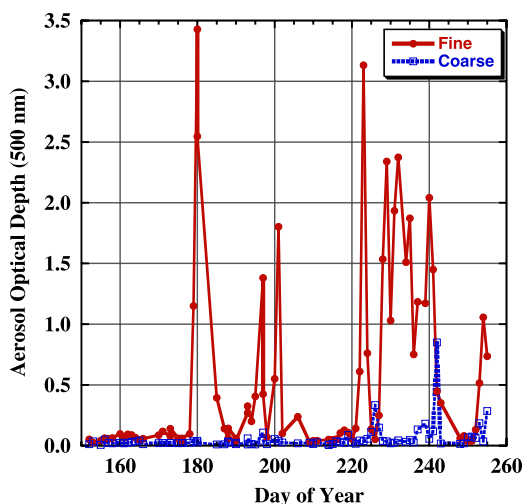


**Figure 6.** Spectral deconvolution algorithm (SDA) computed daily average fine and coarse mode AOD versus day of the year from 1 June 2004 through 12 September 2004 at Bonanza Creek, Alaska.

the low AOD in most years in September (often  $<0.07$ ) leading to higher uncertainty in  $\alpha_{440-870}$ .

### 3.1.2. Daily AOD Variability and Computation of Fine and Coarse Mode AOD

[14] It is noted that there is very large day-to-day variability in AOD at Bonanza Creek in the peak burning season months. For example, during the month of August the daily mean 500 nm AOD varied from 0.05 to 3.2 in 2004 and from 0.03 to 3.3 in 2005 due to variation in source strength and due to the transport, stagnation, and removal effects of regional meteorology.

[15] Based on the assumption that aerosol size distributions are bimodal, O'Neill *et al.* [2001, 2003] have developed a spectral deconvolution algorithm (SDA) that utilizes spectral total extinction AOD data to infer the component fine and coarse mode optical depths. An additional fundamental assumption of the algorithm is that the coarse mode Angstrom exponent and its derivative are both close to zero. The Angstrom exponent  $\alpha$  and the spectral variation of  $\alpha$  (as parameterized by  $\alpha' = d\alpha/d\ln\lambda$ ) are the measurement inputs to the SDA. These continuous-function derivatives (usually computed at a reference wavelength of 500 nm) are derived from a second order fit of  $\ln \tau_a$  versus  $\ln \lambda$  [Eck *et al.*, 1999]. The spectral AODs employed as input to the SDA were limited to the six CIMEL wavelengths ranging from 380 to 1020 nm. Figure 6 shows the time series of fine and coarse mode daily average AOD at 500 nm from the SDA algorithm for 1 June through 12 September 2004 at Bonanza Creek. These are level 2 cloud screened data that have had the SDA algorithm applied to the AOD spectra. It is noted that the coarse mode is typically very low and nearly constant, while the fine mode AOD from biomass burning exhibits very large day-to-day variability. Only 2 days show the coarse mode AOD to be significantly higher than the fine mode, possibly due to dust transported from Asia or from residual cloud contamination. We assume that the fine mode aerosols at Bonanza Creek are dominated by biomass burning smoke since there are numerous fire hot spots observed

(Figure 1), combined with a lack of any other significant regional sources of fine mode particles.

### 3.1.3. Comparison of Alaska Smoke AOD Spectral Characteristics to Smoke at Tropical Biomass Burning Sites

[16] A comparison of the daily average 380–500 nm Angstrom exponents as a function of 500 nm AOD for the Bonanza Creek data of 2004 is shown in Figure 7 versus the AERONET data from the major tropical region biomass burning sites of ABRACOS Hill, Brazil (2002 data; southern Amazonia) and Mongu, Zambia (2004; southern Africa savanna burning region). For all three sites the data for the June through October biomass burning seasons are shown. The 380–500 nm Angstrom is computed from linear regression of  $\ln$  AOD versus  $\ln \lambda$  scale at 380, 440, and 500 nm. Reid *et al.* [1999] have shown from Mie computations, with measured smoke size distribution parameters, that the Angstrom exponent computed at shorter wavelengths ( $<500$  nm) is more sensitive to accumulation mode particle size and distribution width, than Angstrom computed at longer wavelengths. From Figure 7 it is seen that the  $\alpha_{380-500}$  values are much lower for the Bonanza Creek site than for the tropical biomass burning sites. This implies much larger accumulation mode particle size for the Alaska fires than for the tropical biomass burning sites. Similarly, in a comparison of high optical depth smoke cases (AOD(500 nm)  $\sim 2.0$ ), Eck *et al.* [2003a] showed that smoke transported long distance from boreal burning regions (in Quebec and Russia) had larger accumulation mode radius than biomass burning aerosols from Brazil and Zambia. Further evidence for large size accumulation mode aerosol particles for the Alaska fires is presented below in comparisons of fine mode fraction as a function of Ang-

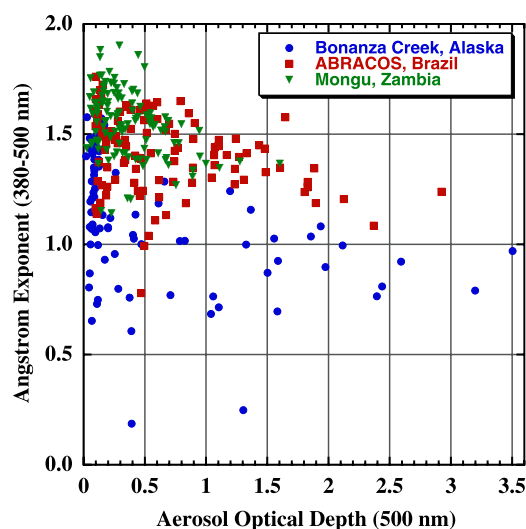


**Figure 7.** A comparison of the daily average 380–500 nm Angstrom exponents as a function of 500 nm AOD for the Bonanza Creek data from 2004 versus the AERONET data from the major tropical region biomass burning sites of ABRACOS Hill, Brazil (2002 data; southern Amazonia) and Mongu, Zambia (2004; southern Africa savanna burning region). For all three sites, the data for the June through October biomass burning seasons are shown.

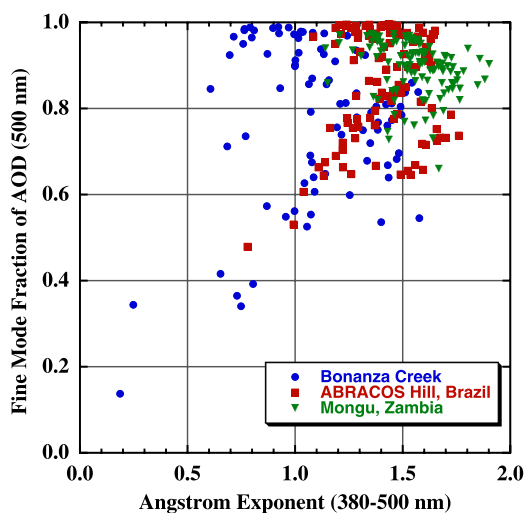


**Figure 8.** Spectral deconvolution algorithm (SDA) computed daily average fine mode fraction (FMF) for the Bonanza Creek site plotted versus  $\alpha_{380-500}$  and compared with measurements made in Brazil and Zambia (from the same observations as shown in Figure 7).

strom exponent and also in section 3.2.1 from the almucantar retrievals of size distribution.

[17] The SDA algorithm computed daily average fine mode fractions (FMF) for the Bonanza Creek site are plotted versus  $\alpha_{380-500}$  in Figure 8, and compared with measurements made in Brazil and Zambia (from the same observations as shown in Figure 7). For the same range of FMF, 0.8–1.0, the  $\alpha_{380-500}$  is typically significantly lower for the Alaska site than the Brazil and Zambia biomass burning sites, again suggesting much larger accumulation mode particles in Alaska. In addition to the greater percentage of smoldering combustion for the forest regions with woody fuels (Alaska and Brazil) other possible reasons for larger accumulation mode particles include higher AOD levels (Figure 7) in Alaska and Brazil that increase the coagulation rate since aerosol concentrations are higher. Another possible factor in creating large accumulation particles might be the characteristics of smoke from peat burning in Alaska [Reid *et al.*, 2005a], since extensive areas of peatlands (in addition to forests) were observed to burn during the summer of 2004.

### 3.2. Retrievals of Aerosol Size Distribution and Single Scattering Albedo in Central Alaska

#### 3.2.1. Volume Size Distributions

[18] The almucantar retrievals of aerosol volume size distributions for the Bonanza Creek site in 2004 and 2005 for scans where AOD(440 nm) > 0.4 are shown in Figure 9a. These averages are plotted as a function of AOD(440 nm) with AOD bins from 0.4–0.8, >0.8–1.2, ..., >2.4–2.8, >2.8 resulting in averages of from 9 to 34 almucantars per bin. At all AOD levels the retrievals show the dominance of fine mode aerosols, and the  $\alpha_{440-870}$  for the bins range from 1.74 at the lowest AOD(440) average of 0.53 to 1.36 at the highest AOD bin of 3.15. If one defines an effective upper limit of the fine mode distribution as some appropriate fraction of the peak then one can observe a shifting of this upper limit as AOD increases (consistent with the decrease

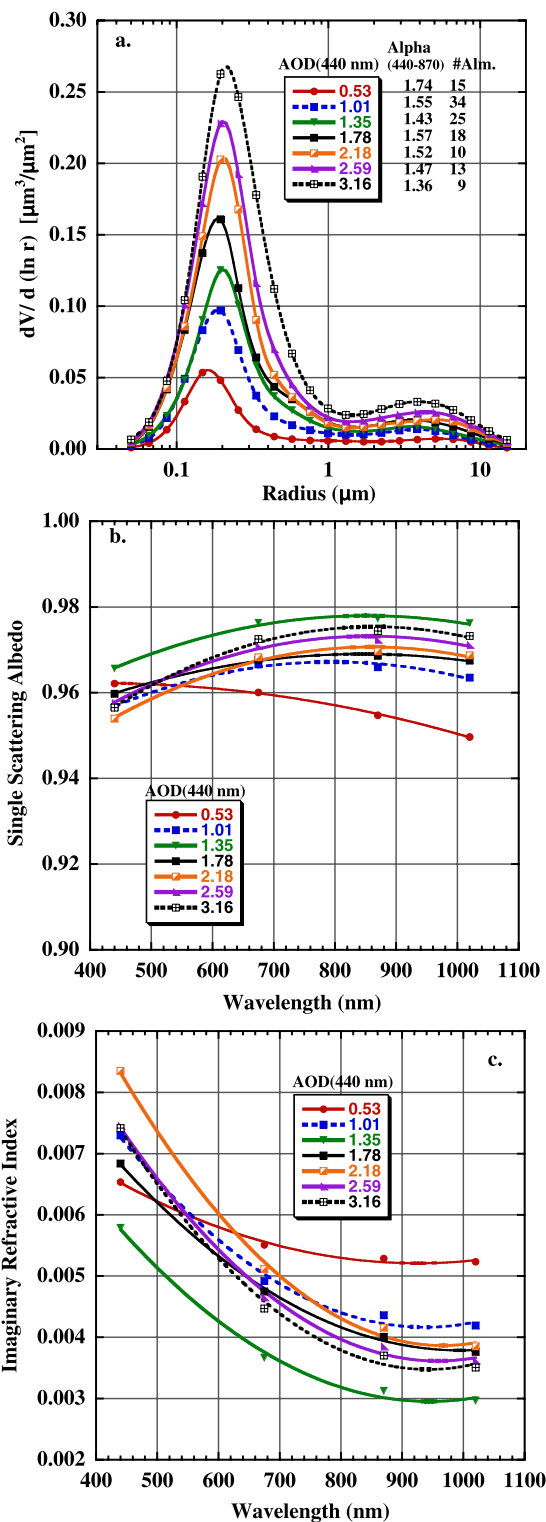


**Figure 9.** Almucantar retrievals of (a) aerosol volume size distributions, (b) single scattering albedo, and (c) imaginary part of the refractive index from the Bonanza Creek site in 2004 and 2005 for scans where AOD(440 nm) > 0.4. These averages are plotted as a function of AOD(440 nm) for AOD bins at 0.4–0.8, >0.8–1.2, >1.2–1.6, ..., >2.4–2.8, >2.8 resulting in averages of from 9 to 34 almucantar scans per bin.

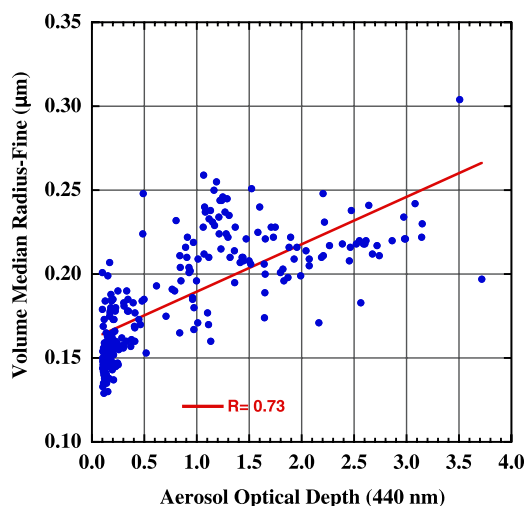


**Figure 10.** Fine mode volume median radius versus AOD(440 nm) at Bonanza Creek (2004 and 2005), showing a general increase in volume median radius as AOD increases ( $r^2 = 0.53$ ).

in Angstrom exponent), with the nearly lognormal fine mode distributions extending to 1 micron radius at the higher AOD levels accompanied by a relatively insignificant (optically) coarse mode at all AOD levels. The lack of a significant coarse mode is typical of biomass burning aerosols at moderate to high AOD from other major source regions such as Amazonia and southern Africa [Schafer *et al.*, 2008; Reid *et al.*, 2005a; Eck *et al.*, 2001].

[19] Volume median radius of the fine mode ( $r_v$ ) is shown plotted as a function of AOD at 440 nm in Figure 10. Only data where AOD(440) > 0.1 are shown to exclude background aerosol cases and observations that are not related to biomass burning. In calculating  $r_v$ , the maximum radius of the fine mode volume distribution was defined as the minimum between the fine and coarse modes in the retrieved size distribution, over the maximum defined range limits of 0.44 to 0.99  $\mu\text{m}$  radius. The minimum radius for the fine mode is fixed at 0.05  $\mu\text{m}$  radius, which is the minimum radius of the almucentar inversion. Figure 10 shows that there is a general increase in volume median radius as AOD increases ( $r^2 = 0.53$ ) from  $\sim 0.17 \mu\text{m}$  at low AOD ( $\sim 0.15$  at 440 nm) to a radius approaching  $\sim 0.25 \mu\text{m}$  at very high AOD (AOD = 3). These are very large accumulation mode radius particles, especially compared to biomass burning aerosols in Amazonia and southern Africa where median radius at high AOD (>1.5 at 440 nm) is approximately 0.17  $\mu\text{m}$  [Eck *et al.*, 2001; Reid *et al.*, 2005a; Schafer *et al.*, 2008]. Other boreal biomass burning events with very high AOD ( $\sim 2$  at 500 nm), and therefore high concentrations, also had large radius accumulation mode particles, with long distance transported smoke from a Canadian fire exhibiting  $r_v \sim 0.21 \mu\text{m}$  and transported smoke from a Russian peat/forest fire showing retrieved  $r_v$  of 0.28  $\mu\text{m}$  (Version 2 retrievals as compared to somewhat smaller radius values reported from Version 1 by Eck *et al.* [2003a]). These however were aged aerosol events with smoke age >2 days due to long distance transport from distinct source regions. However, AERONET measurements made in Moscow on 7 September 2002 (AOD(440)

$\sim 2.5$ ) near to a fire that was predominately burning peat had large accumulation mode particles of  $\sim 0.22 \mu\text{m}$  radius despite relatively short transport distance and therefore likely little aging. Therefore the large radius of the smoke aerosol measured in late summer in Alaska in 2004 and 2005 possibly resulted in part from the smoldering combustion of peat fuels in addition to the high aerosol concentrations that would result in greater coagulation, condensation and secondary production rates.

[20] In comparison to the Alaska smoke we show the aerosol volume size distribution retrievals for biomass burning aerosols from the Mongu, Zambia AERONET site in Figure 11a. These Mongu retrievals are from September (peak burning month) data only for the years 1997–2005, and shown for two AOD levels,  $\sim 0.5$  and  $\sim 1.3$  at 440 nm. Both the mean sizes and the shift of fine mode radius as AOD increases in Zambia are relatively small (radius  $\sim 0.14$  to  $0.16 \mu\text{m}$ ) as compared to the boreal smoke measured in Alaska. Smoke in Brazil (southern Amazonia; not shown) exhibited slightly larger fine mode radius ( $\sim 0.15$  to  $0.17 \mu\text{m}$  [Schafer *et al.*, 2008]) at these AOD levels than Zambia, possibly due to more smoldering combustion of woody fuels and higher aerosol concentrations that may have lead to greater coagulation rates. In addition to the relatively small change in volume median radius in Mongu, Zambia, the width of the fine mode size distribution is narrower for the Zambia smoke than for the Alaska smoke. The geometric standard deviation for the Zambia smoke ranges from  $\sim 1.47$  to  $1.51$ , while for the Alaska smoke in 2004 and 2005 it ranges from  $\sim 1.66$  to  $1.79$ . The causes of these large regional differences in biomass burning aerosol size distributions are most likely differences both in fuel characteristics and in the predominant phases of combustion. In the Zambian savanna environment, grasses are a dominant fuel type and this typically burns relatively rapidly with a high proportion of the combustion in the flaming phase [Ward *et al.*, 1996]. This contrasts with Alaska forests where intense rapid crown fires burn predominately in the flaming phase often followed by long periods of smoldering combustion of the woody fuels and smoldering of organic soil and peat layers. Reid and Hobbs [1998] measured larger smoke particle radius for smoldering phase emissions than for flaming phase in Amazonia. Therefore in Alaska it is possible that a combination of aerosol sizes produced from intense crown flaming combustion and extensive smoldering combustion of wood and peat, combined with coagulation from very high concentrations, have produced wider fine mode size distributions.

### 3.2.2. Spectral Single Scattering Albedo

[21] The average spectral single scattering albedo as a function of AOD, for cases with AOD(440 nm) > 0.4, for the Bonanza Creek site are shown in Figure 9b. These are the same almucentar scans as are shown for the size distributions retrievals in Figure 9a. Leahy *et al.* [2007] have shown excellent agreement between airborne in situ measured  $\omega_0$  at 550 nm and AERONET version 2 retrievals for southern African savanna biomass burning aerosols, with a mean discrepancy of  $-0.01$  for 5 coincident flights over AERONET sites.

[22] The average single scattering albedo in 2004 and 2005 at Bonanza Creek is high (weak absorption) for biomass burning aerosols, with most values ranging from  $\sim 0.96$  to  $0.97$  (Figure 9b). Only four of the individual retrievals out of

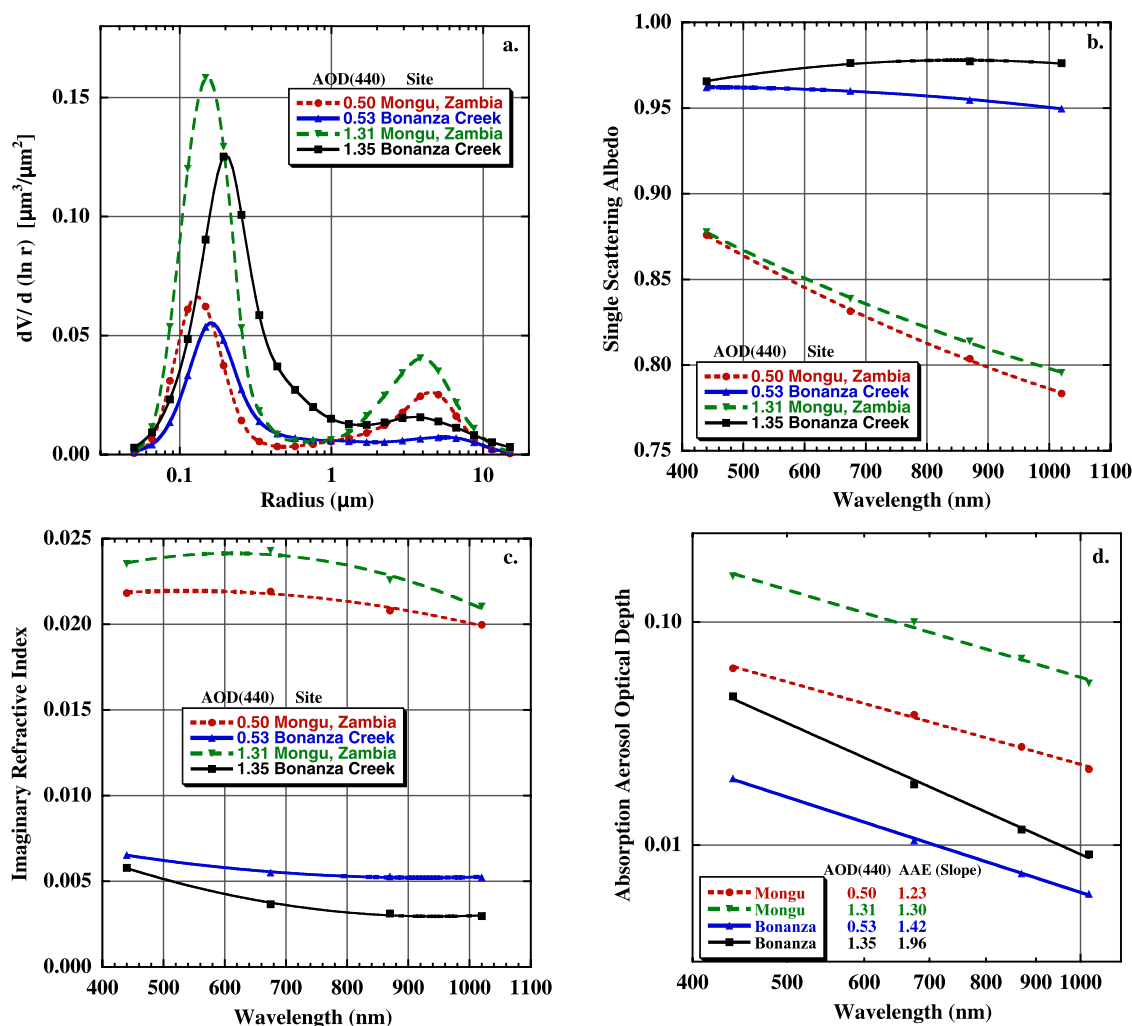


**Figure 11.** Almucantar retrievals of (a) aerosol volume size distributions, (b) single scattering albedo, and (c) imaginary part of the refractive index and (d) absorption aerosol optical depth from the Mongu, Zambia AERONET site compared to Bonanza Creek for scans where AOD(440 nm) > 0.4. The Mongu retrievals are from September (peak biomass burning month) data only for the years 1997–2005, for a total of 506 almucantar retrievals.

a total of 124 almucantars with AOD(440 nm) > 0.4 in 2004 and 2005 had  $\omega_0$  less than 0.935 at 440 nm, with the lowest at 0.909. The highest retrieved value of  $\omega_0$  at 440 nm is slightly lower (by  $\sim 0.01$ ) than that at 675 nm, and the  $\omega_0$  from 675 nm through 1020 nm are relatively constant (Figure 9b). This spectral dependence of  $\omega_0$  appears to be anomalous for biomass burning aerosols, as the single scattering albedo typically decreases with increasing wavelength in both measurements and retrievals [Reid *et al.*, 2005b]. For example, Dubovik *et al.* [2002] show this typical wavelength dependence for biomass burning aerosols from four major regions: Amazonian forest, S. American cerrado (savanna-like), African savanna in Zambia, and boreal forest (primarily Canada). However, the boreal forest data set in Dubovik *et al.* [2002] does not include events with as high AOD as occurred in Alaska in 2004 and 2005, nor does it include observations with significant peat burning. For all other years from 1994–2007 (excluding 2004 and 2005) there were a total of only 14 almucantar retrievals at Bonanza Creek with AOD(440 nm) > 0.4. Two of these had

$\omega_0$  at 440 nm of  $\sim 0.86$  which suggests flaming phase crown fires, while the other 12 had values ranging from 0.92 to 0.98. The mean of these 14 almucantars was 0.94 at 440 nm and within less than 0.005 of the values given by Dubovik *et al.* [2002] at all 4 wavelengths (Dubovik's values were a mean for boreal forest biomass burning aerosols).

[23] Similar wavelength dependence of  $\omega_0$  to the Alaskan smoke of 2004 and 2005 was observed however for the previous mentioned case of peat burning smoke in Moscow on 7 September 2002 at high AOD (average of 2.45 at 440 nm). For this case the  $\omega_0$  was relatively constant with wavelength at  $\sim 0.95$ – $0.96$  (average of 6 almucantar retrievals) with the 440 nm  $\omega_0$  value  $\sim 0.01$  lower than at 675 nm and nearly constant from 675 to 1020 nm. Furthermore, the average spectral dependence of the imaginary refractive index (0.0078, 0.0052, 0.0042, 0.0038 for 440, 675, 870 and 1020 nm respectively) was very similar to that observed for the Alaskan smoke (Figure 9c).

[24] The typical single scattering albedo wavelength dependence of biomass burning aerosols (decreasing  $\omega_0$  as  $\lambda$  increases) is due to a relatively constant spectral imagi-

nary refractive index coupled with small size fine mode particles [Bergstrom *et al.*, 2002; Eck *et al.*, 2003b]. The relatively constant imaginary refractive index results from the dominance of black carbon in the aerosol absorption. As an example of high black carbon fraction biomass burning aerosol, Figures 11b and 11c present comparisons to AERONET version 2 retrievals from Mongu, Zambia for September (peak burning month) showing the steep linear decrease in  $\omega_0$  as wavelength increases and the relatively constant imaginary refractive index ( $k$ ) as a function of wavelength. However, the imaginary refractive index of the Alaska smoke observations shows low values (weak absorption) implying small black carbon fraction, and a large relative increase at 440 nm (small in absolute magnitude however; Figure 9c) which may result from additional absorption by organic carbon. Kirchstetter *et al.* [2004] present spectral imaginary refractive indices for organic carbon and for black carbon. Although the imaginary refractive indices ( $k$ ) they give for organic carbon (0.063 at 450 nm) are high relative to what we retrieved for the Alaska smoke, the spectral dependence shows a rapid increase as wavelength decreases from 700 nm to 450 nm, while black carbon  $k$  remains much higher and relatively constant ( $\sim 0.72$ ). For the burning of lignite fuel Bond *et al.* [1999] also measured greater fine particle absorption at shorter wavelengths (450 nm), implying larger imaginary refractive index at shorter wavelengths, possibly due to absorption by organic carbon. It is noted that their laboratory combustion of this lignite fuel occurred partially in the smoldering phase. However, it is noted that the absorption properties of organic carbon are not well known and therefore are a topic of much recent research.

[25] Another factor that contributes to the relatively constant spectral single scattering albedo of the Alaskan smoke is the much larger size and wider distribution of the fine mode particle radius, as compared to particles from most other biomass burning regions. Because the scattering cross section (or hence scattering optical depth) increases more rapidly than absorption cross section with increasing particle size the  $\omega_0$  also increases (in the absence of variations in refractive index) with increasing particle size. This trend is the optical equivalent of stating (as above) that  $\omega_0$  typically decreases with increasing wavelength. However, this trend is less extreme at larger particle sizes because the  $\omega_0$  approaches unity at a lesser rate with respect to increasing particle size (or decreasing wavelength).

[26] In situ measurements from nephelometer and particle soot absorption photometer data at the surface in Barrow, Alaska on 3–4 July 2004 yielded an aerosol single scattering albedo of 0.96 at 550 nm [Stohl *et al.*, 2006; Stone *et al.*, 2008], for a case of very high smoke AOD advected from fires in central Alaska and the Yukon. This is essentially equal to the mean AERONET retrievals of  $\omega_0$  interpolated to 550 nm for the total column aerosol in central Alaska at Bonanza Creek (Figure 9a). For agricultural smoke originating in Europe and subsequently advected to Svalbard in the Arctic, Myhre *et al.* [2007] computed a single scattering albedo of 0.98 at 440 nm based on in situ surface based aerosol chemical composition, suggesting that the aerosol may have become less absorbing after transport and aging.

[27] The spectral aerosol absorption optical depths (AAOD) computed from the measured AOD and retrieved

$\omega_0$  from 440 to 870 nm are compared in Figure 11d for the smoke in southern Africa versus the Alaska smoke in 2004 and 2005 (these are from the same observations as shown in Figures 11a, 11b, and 11c). The AERONET inferred spectral AAOD are very linear with wavelength in Figure 11d, similar to linearity noted by Bergstrom *et al.* [2007] in five different field experiment campaigns. The negative of the slope of the absorption optical depth with wavelength in logarithmic coordinates defines the Absorption Angstrom Exponent (AAE). Values of the AAE for the Mongu, Zambia smoke range from 1.23 to 1.30, similar to the value of 1.45 shown by Bergstrom *et al.* [2007] for the SAFARI 2000 experiment (which included Zambia in the study region) biomass burning aerosols for the similar wavelength range of 325 to 1000 nm. These relatively low values of AAE are typical for aerosol absorption largely dominated by black or light absorbing carbon. For the Alaska smoke the value of AAE was 1.42 at the lower AOD (440 nm) of 0.53 while at the higher AOD of 1.35 the AAE increased to 1.96. The increase of the AAE at higher AOD (similar values of AAE up to 2.07 were computed for AOD from 1.35 to 3.15 at 440 nm at Bonanza Creek) suggests absorption by different material. This suggests that on average the Alaska smoke absorption in these years possibly shifted from domination by black carbon at lower AOD levels to an increasing influence of absorption by other materials, most likely organic carbon, at higher AOD. For smoke produced by combustion of various fuels, measured in controlled laboratory conditions, Lewis *et al.* [2008] measured AAE as high as 2.5 (532 to 870 nm) at high  $\omega_0$  (near unity) while AAE values approached 1.0 for  $\omega_0 < 0.8$  at 532 nm. The measured organic carbon fraction to total carbon was highest for the smoke with the highest AAE and  $\omega_0$ , thereby suggesting that the enhanced absorption AAE results from light absorbing organic carbon.

### 3.3. Seasonal Variation of AOD in the Coastal Arctic at Barrow, Alaska

[28] In this section we present data from the Arctic AERONET site located at Barrow, Alaska on the Beaufort Sea coast (Figure 1). The data collection at this site has many more gaps than for the Bonanza Creek site in central Alaska due to its more severe weather, which sometimes resulted in instrument electronic or mechanical problems. This occurred especially in earlier years before a modified version of the CIMEL that incorporated heating elements was deployed. Additionally there is more persistent cloud cover at this site than at Bonanza Creek, resulting in fewer observations of the sun, therefore less AOD measurements and very few almucantar scans of sky radiance distribution. Data were acquired in 1999, 2002, 2004, 2005, 2006, 2007, and 2008 however measurements were made during the peak Arctic haze month of April in only three years, 2002, 2005 and 2008, when data collection began in late March or early April. All years had monitoring from July through September, and four of the six years had data from May through September, thus covering the biomass burning season. Therefore due to the numerous gaps in data acquisition, the AERONET data presented here for Barrow cannot be considered a fully representative monitoring record, especially for the spring arctic haze season. These

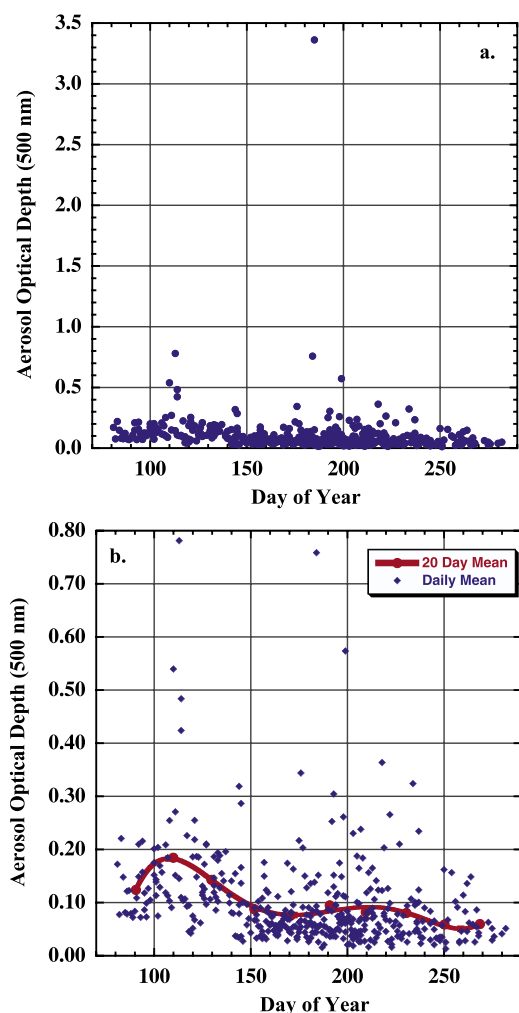


**Figure 12.** (a) The daily average 500 nm AOD measured at the Barrow AERONET site as a function of the day of the year for all monitoring during the 1999 through 2008 time interval. (b) The same as in Figure 12a, but with the single outlier point of AOD (500 nm) of 3.4 from 3 July 2004 removed and with 20-day averages computed.

data gaps therefore preclude any analysis of trends. However, these data still provide some measure of the seasonality of AOD in Arctic Alaska.

[29] Due to the persistent high cloud fractions and also sometimes homogeneous nature of the Arctic clouds, cloud screening is particularly challenging at the Barrow site. Therefore in addition to the standard AERONET cloud screening [Smirnov *et al.*, 2000], we have also set a threshold of Angstrom Exponent (440–870 nm)  $>0.75$  to exclude cases of contamination from spatially homogeneous clouds. The  $\alpha_{440-870}$  threshold of  $>0.75$  corresponds to a fine mode fraction of the AOD of greater than  $\sim 50\%$  [Eck *et al.*, 2005]. However, application of this threshold excludes coarse mode dust aerosol events of Asian dust transported across the northern Pacific [Stone *et al.*, 2007]. Since we are focusing on biomass burning and Arctic haze that are both accumulation mode aerosols, this additional screening does not affect the analysis of these types of aerosols.

[30] Figure 12 shows the daily average 500 nm AOD measured at Barrow as a function of the day of the year for all monitoring during the 1999 through 2008 time interval. In Figure 12a there is one outlier point at the extremely high AOD of 3.4 that occurred at 23 UTC on 3 July 2004 (the next highest daily mean value was 0.78). The Angstrom exponent for this extreme case was 1.51, thus this was a fine mode dominated event and in the same range of  $\alpha$  values as the high AOD smoke events occurring in central Alaska (Bonanza Creek, see Figure 3b). Stohl *et al.* [2006] discuss this same event on 3–4 July 2004 and indicate that the NOAA four-channel sunphotometer at Barrow was completely attenuated on this date and time and that the 500 nm AOD probably exceeded 3 when the 500 nm channel measurement was near zero, and may have even exceeded 4 or 5 when all channels were completely attenuated, due to the combination of high AOD and large solar zenith angle. Stohl *et al.* [2006] have shown from transport modeling that this smoke event originated from the fires located in central Alaska and the Canadian Yukon, and that the smoke continued to be transported beyond Barrow and deep into the arctic. Their simulations suggested that smoke from this event reached the North Pole on 8 July 2004 although cloud cover precluded verification from satellite images. The AERONET site located at Resolute Bay, Canada ( $74^{\circ}44'N$ ,  $94^{\circ}54'W$ ;  $\sim 1950$  km ENE from Barrow) measured smoke AOD on 5 July 2004 as high as 2.3 at 500 nm ( $\alpha_{440-870} > 1.3$ ) from this same arctic transport event. A Terra MODIS image [Stohl *et al.*, 2006, Figure 7] shows widespread smoke from Alaska and the Yukon through the Arctic islands of Canada on 5 July 2004.

[31] Figure 12b is the same as 12a but with the extreme AOD event of 3 July 2004 excluded. Individual daily averages of AOD(500 nm) are shown as well as 20 day interval means (means computed with the one extreme day removed also). Seasonality of AOD is evident, with the highest 20-day averages of AOD occurring during the arctic haze season from late March through mid-May. These higher average AOD values result partly from the lack of measured low background AOD in the spring, when values are rarely lower than 0.07. In contrast, the daily average AOD during summer months is often  $<0.04$  and as low as 0.02. However, daily average AOD on some summer days, as high as or higher than the spring Arctic haze AOD, from biomass burning aerosols result in mean values of AOD during the summer that are elevated significantly above background levels. Again it is emphasized that due to a much less extensive data record at Barrow (as compared to Bonanza Creek), and since the extreme Alaska burning years of 2004 and 2005 are included, that both the spring and summer season means may not be truly representative of the long term mean at Barrow.

[32] The three 20-day means from late March through mid-May computed primarily from 2002, 2005, and 2008 data yield a 60-day mean 500 nm AOD of  $\sim 0.150$  during the arctic haze period, as compared to a summer months average of  $\sim 0.085$ . Peak months of arctic haze occurrences are March, April, and May as determined by aircraft visual observations (summarized by Shaw [1995]) and from ground-based photometer observations [Herber *et al.*, 2002]. Engvall *et al.* [2008] suggest that the rapid transition in the arctic from accumulation mode dominated aerosol in

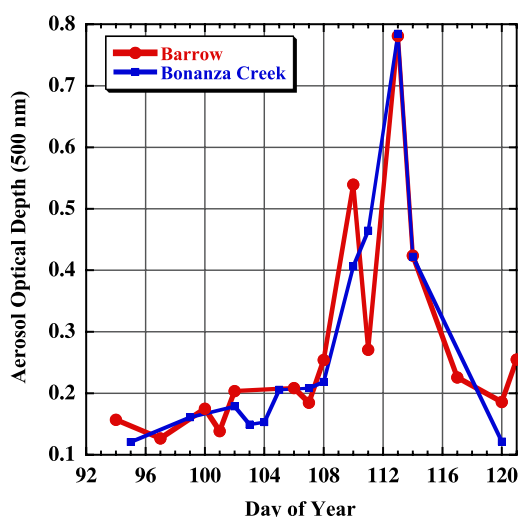


**Figure 13.** The daily average 500 nm AOD measured at both the Barrow and Bonanza Creek AERONET sites as a function of the day of the year for April 2008. The April 2008 monthly mean AOD were equal at both sites, 0.28 at 500 nm.

spring to Aitkin mode dominated in summer is not due to transport alone. Their simulations suggest that this rapid transition may result from a balance between incident solar radiation, transport, and condensational sink processes.

[33] Smoke that originates from biomass burning in both North America (Alaska and Canada) and Siberia affect the aerosol optical depth in Alaska. In April 2008, *Warneke et al.* [2009] measured in situ chemical characteristics from aircraft of many smoke plumes over northern Alaska that originated predominately from forest fires in southern Siberia, but also from agricultural burning in Kazakhstan and Eastern Europe. Due to low snow amount, the forest fire season started unusually early in Siberia in 2008. The daily mean AOD data for April 2008 from both the Barrow and Bonanza Creek sites ( $\sim 800$  km apart) are shown in Figure 13. High AOD values of almost the same magnitude were observed on most days at both sites, showing the extensive and relatively uniform extent of this primarily smoke haze in central and northern Alaska. In fact, the April 2008 monthly mean AOD at both Barrow and Bonanza Creek were equal, 0.28 at 500 nm, with high monthly average Angstrom Exponent (440–870 nm) at both sites, 1.25 at Barrow and 1.10 at Bonanza Creek.

[34] *Shaw* [1982] measured AOD from sunphotometer at Barrow during the mid to late 1970s and computed a March–April mean of 0.135 at 500 nm. Therefore the mean AOD measured by AERONET for the spring arctic haze (and smoke) at Barrow for 2002, 2005 and 2008 were somewhat higher than that measured  $\sim 25$  years earlier. *Bodhaine and Dutton* [1993] presented measurements of AOD at Barrow computed from broadband (300–690 nm) pyrliometer measurements for the years 1977–1992, with estimates of volcanic aerosol optical depth removed. They show relatively low AOD in 1980 and 1981 and a significant downward trend from 1982 (peak year) to 1992 that they suggest may have resulted from the reduction of emissions in the Soviet Union and Europe during that era.

Continued monitoring of AOD at Barrow is important for understanding arctic haze magnitude and trends. Ground based photometric measurements of AOD at 532 nm at the arctic island of Spitsbergen ( $\sim 79^{\circ}\text{N}$ ,  $12^{\circ}\text{E}$ ) by *Herber et al.* [2002] from 1991 through 1999 showed a gradual increase in AOD of  $\sim 9\%$  over the 9 year interval. The relative sparseness of long-term records of AOD at Arctic locations coupled with the possibility of different regional influences (sources and meteorology) make it very difficult to assess trends of aerosol loading across the entire arctic region.

#### 4. Summary and Conclusions

[35] Aerosol optical properties data acquired from monitoring at two AERONET sites in Alaska were investigated. Data from long-term monitoring at a central Alaska boreal forest region site (Bonanza Creek) and seasonal monitoring at a coastal site on the Arctic Ocean (Barrow) were analyzed.

[36] 1. Measurements of AOD at Bonanza Creek from 1994 through 2008 showed extreme interannual variability that resulted from episodic major forest fire emissions in dry years as compared to background levels during wet years. Record forest burning extent in the years 2004 and 2005 resulted in monthly average AOD in August of both years that was similar to peak burning season monthly mean AOD in major biomass burning regions in Brazil and Zambia.

[37] 2. Both almucantar retrieved aerosol size distributions and Angstrom exponent values at Bonanza Creek were consistent in identifying the fine mode particles in the major burning years of 2004 and 2005 as being significantly larger than for smoke aerosol in tropical burning regions. The retrieved volume size distribution median radius typically ranged from  $\sim 0.20$  to  $0.25 \mu\text{m}$  for observations when AOD  $> 1.0$  at 440, as compared to  $\sim 0.17 \mu\text{m}$  for AERONET retrievals of biomass burning aerosols at the same AOD levels in Brazil and Zambia. Additionally the width of the fine mode distribution at Bonanza Creek was broader, with the geometric standard deviation of  $\sim 1.66$  to  $\sim 1.79$  as compared to  $\sim 1.5$  at major tropical biomass burning region sites. The significantly broader distribution may possibly be due to several factors including increased coagulation rates at very high AOD for aged aerosol along with continued emission of fresh (smaller) particles from numerous fires, and also possible differences in particle size from smoldering combustion partly from peat fires.

[38] 3. Absorption by the smoke aerosol in Bonanza Creek in 2004 and 2005 was very weak, with retrieved single scattering albedo ranging from  $\sim 0.96$  to  $0.97$ , along with relatively flat spectral dependence. These high single scattering albedos result from small values of the imaginary index of refraction, implying low black carbon fraction probably due to predominately smoldering combustion, coupled with large fine mode particle radius which results in greater scattering efficiency (increased  $\omega_0$  amplitude) and reduced wavelength dependence of the  $\omega_0$ . Additionally, the single scattering albedo at 440 nm was  $\sim 0.01$  lower than at the longer wavelengths due to a somewhat larger imaginary refractive index at 440 nm, which is possibly due to enhanced short wavelength absorption by organic carbon aerosols. This also suggests the possibility that smoke from

peat burning (smoldering combustion) had a significant influence on aerosol emissions.

[39] 4. Although AERONET monitoring at the Arctic coastal site of Barrow from 1999 to 2008 was often interrupted and not complete enough to be considered a representative climatology, some seasonal characteristics of AOD were nonetheless evident. The average AOD in the spring (late March through late May) is higher than the average AOD in the summer. Even though several individual daily mean values in summer are significantly higher (from transported biomass burning smoke) than most daily means in spring, the lack of very low background AOD levels in spring, due primarily to persistent industrial arctic haze, resulted in higher mean AOD in spring.

[40] **Acknowledgments.** This project was supported by Michael D. King, retired in 2008 from the NASA EOS project office, and by Hal B. Maring, Radiation Sciences Program, NASA Headquarters. We thank the site managers at the Bonanza Creek site (currently Jamie Hollingsworth, University of Alaska Fairbanks) and the Barrow site (currently Walter Brower and Jimmy Ivanoff) for their diligence over the years in operating and maintaining the AERONET instrumentation. Bernie Zak was the coordinator and Rick Wagener was the principal investigator for the Barrow AERONET site. Drs. Reid and Hyer's participation was funded by the NASA Interdisciplinary Science Program and the Office of Naval Research Code 32. We also thank the anonymous reviewers for comments that resulted in improvements in the manuscript. This paper is dedicated to the memory of Wayne Newcomb (1952–2008) of the NASA AERONET project, whose ability to keep AERONET sites working through his combination of extensive knowledge, timely communication, and good humor will never be forgotten.

## References

- Bergstrom, R. W., P. B. Russell, and P. Hignett (2002), Wavelength dependence of the absorption of black carbon particles: Predictions and results from the TARFOX experiment and implications for the aerosol single scattering albedo, *J. Atmos. Sci.*, **59**, 567–577.
- Bergstrom, R. W., P. Pilewskie, P. B. Russell, J. Redemann, T. C. Bond, P. K. Quinn, and B. Sierau (2007), Spectral absorption properties of atmospheric aerosols, *Atmos. Chem. Phys.*, **7**, 5937–5943.
- Bodhaine, B. A., and E. G. Dutton (1993), A long-term decrease in Arctic haze at Barrow, Alaska, *Geophys. Res. Lett.*, **20**(10), 947–950.
- Bonan, G. B., and H. H. Shugart (1989), Environmental factors and ecological processes in boreal forests, *Annu. Rev. Ecol. Syst.*, **20**, 1–28.
- Bond, T. C., T. L. Anderson, and D. Campbell (1999), Calibration and intercomparison of filter-based measurements of visible light absorption by aerosols, *Aerosols Sci. Technol.*, **30**, 582–600.
- Dubovik, O., and M. D. King (2000), A flexible inversion algorithm for the retrieval of aerosol optical properties from Sun and sky radiance measurements, *J. Geophys. Res.*, **105**(D16), 20,673–20,696.
- Dubovik, O., A. Smirnov, B. N. Holben, M. D. King, Y. J. Kaufman, T. F. Eck, and I. Slutsker (2000), Accuracy assessments of aerosol optical properties retrieved from AERONET Sun and sky-radiance measurements, *J. Geophys. Res.*, **105**(D8), 9791–9806.
- Dubovik, O., B. N. Holben, T. F. Eck, A. Smirnov, Y. J. Kaufman, M. D. King, D. Tanre, and I. Slutsker (2002), Variability of absorption and optical properties of key aerosol types observed in worldwide locations, *J. Atmos. Sci.*, **59**, 590–608.
- Dubovik, O., et al. (2006), Application of spheroid models to account for aerosol particle nonsphericity in remote sensing of desert dust, *J. Geophys. Res.*, **111**, D11208, doi:10.1029/2005JD006619.
- Eck, T. F., B. N. Holben, J. S. Reid, O. Dubovik, A. Smirnov, N. T. O'Neill, I. Slutsker, and S. Kinne (1999), Wavelength dependence of the optical depth of biomass burning, urban, and desert dust aerosols, *J. Geophys. Res.*, **104**(D24), 31,333–31,349.
- Eck, T. F., B. N. Holben, D. E. Ward, O. Dubovik, J. S. Reid, A. Smirnov, M. M. Mukelabai, N. C. Hsu, N. T. O'Neill, and I. Slutsker (2001), Characterization of the optical properties of biomass burning aerosols in Zambia during the 1997 ZIBBEE Field Campaign, *J. Geophys. Res.*, **106**(D4), 3425–3448.
- Eck, T. F., B. N. Holben, J. S. Reid, N. T. O'Neill, J. S. Schafer, O. Dubovik, A. Smirnov, M. A. Yamasoe, and P. Artaxo (2003a), High aerosol optical depth biomass burning events: A comparison of optical properties for different source regions, *Geophys. Res. Lett.*, **30**(20), 2035, doi:10.1029/2003GL017861.
- Eck, T. F., et al. (2003b), Variability of biomass burning aerosol optical characteristics in southern Africa during the SAFARI 2000 dry season campaign and a comparison of single scattering albedo estimates from radiometric measurements, *J. Geophys. Res.*, **108**(D13), 8477, doi:10.1029/2002JD002321.
- Eck, T. F., et al. (2005), Columnar aerosol optical properties at AERONET sites in central eastern Asia and aerosol transport to the tropical mid-Pacific, *J. Geophys. Res.*, **110**, D06202, doi:10.1029/2004JD005274.
- Eck, T. F., et al. (2008), Spatial and temporal variability of column-integrated aerosol optical properties in the southern Arabian Gulf and United Arab Emirates in summer, *J. Geophys. Res.*, **113**, D01204, doi:10.1029/2007JD008944.
- Engvall, A.-C., R. Krejci, J. Strom, R. Treffeisen, R. Scheele, O. Hermansen, and J. Paatero (2008), Changes in aerosol properties during spring-summer period in the Arctic troposphere, *Atmos. Chem. Phys.*, **8**, 445–462.
- Flanner, M. G., C. S. Zender, J. T. Randerson, and P. J. Rasch (2007), Present-day climate forcing and response from black carbon in snow, *J. Geophys. Res.*, **112**, D11202, doi:10.1029/2006JD008003.
- Flannigan, M. D., K. A. Logan, B. D. Amiro, W. R. Skinner, and B. J. Stocks (2005), Future area burned in Canada, *Clim. Change*, **72**, 1–16.
- Generoso, S., I. Bey, J.-L. Attié, and F.-M. Bréon (2007), A satellite- and model-based assessment of the 2003 Russian fires: Impact on the Arctic region, *J. Geophys. Res.*, **112**, D15302, doi:10.1029/2006JD008344.
- Hansen, J., and L. Nazarenko (2004), Soot climate forcing via snow and ice albedos, *Proc. Natl. Acad. Sci.*, **101**(2), 423–428.
- Herber, A., L. W. Thomason, H. Gernandt, U. Leiterer, D. Nagel, K. H. Schulz, J. Kaptur, T. Albrecht, and J. Notholt (2002), Continuous day and night aerosol optical depth observations in the Arctic between 1991 and 1999, *J. Geophys. Res.*, **107**(D10), 4097, doi:10.1029/2001JD000536.
- Holben, B. N., et al. (1998), AERONET — A federated instrument network and data archive for aerosol characterization, *Remote Sens. Environ.*, **66**, 1–16.
- Holben, B. N., T. F. Eck, I. Slutsker, A. Smirnov, A. Sinyuk, J. Schafer, D. Giles, and O. Dubovik (2006), AERONET's Version 2.0 quality assurance criteria, in *Remote Sensing of Atmosphere and Clouds*, edited by S.-C. Tsay et al., *Proc. SPIE*, **6408**, 64080Q, doi:10.1117/12.706524.
- Intergovernmental Panel on Climate Change (IPCC) (2007), *Climate Change 2007: The Physical Science Basis*, in *Contribution of Working Group I to the Fourth Assessment Report of the Intergovernmental Panel on Climate Change*, edited by S. Solomon et al., 996 pp., Cambridge Univ. Press, Cambridge, U. K.
- Justice, C. O., L. Giglio, S. Korontzi, J. Owens, J. T. Morissette, D. Roy, J. Descloitres, S. Alleaume, F. Petitcolin, and Y. Kaufman (2002), The MODIS fire products, *Remote Sens. Environ.*, **83**, 244–262.
- Kasischke, E. S., and M. R. Turetsky (2006), Recent changes in the fire regime across the North American boreal region: Spatial and temporal patterns of burning across Canada and Alaska, *Geophys. Res. Lett.*, **33**, L09703, doi:10.1029/2006GL025677.
- Kasischke, E. S., D. Williams, and D. Barry (2002), Analysis of the patterns of large fires in the boreal forest region of Alaska, *Int. J. Wildland Fire*, **11**(2), 131–144.
- Kharuk, V. I., K. J. Ranson, and M. L. Dvinskaya (2008), Wildfires dynamic in the larch dominance zone, *Geophys. Res. Lett.*, **35**, L01402, doi:10.1029/2007GL032291.
- Kirchstetter, T. W., T. Novakov, and P. V. Hobbs (2004), Evidence that the spectral dependence of light absorption by aerosols is affected by organic carbon, *J. Geophys. Res.*, **109**, D21208, doi:10.1029/2004JD004999.
- Leahy, L. V., T. L. Anderson, T. F. Eck, and R. W. Bergstrom (2007), A synthesis of single scattering albedo of biomass burning aerosol over southern Africa during SAFARI 2000, *Geophys. Res. Lett.*, **34**, L12814, doi:10.1029/2007GL029697.
- Lewis, K., W. P. Arnott, H. Moosmüller, and C. E. Wold (2008), Strong spectral variation of biomass smoke light absorption and single scattering albedo observed with a novel dual-wavelength photoacoustic instrument, *J. Geophys. Res.*, **113**, D16203, doi:10.1029/2007JD009699.
- McConnell, J. R., R. Edwards, G. L. Kok, M. G. Flanner, C. S. Zender, E. S. Saltzman, J. R. Banta, D. R. Pasteris, M. M. Carter, and J. D. W. Kahl (2007), 20th-Century Industrial Black Carbon Emissions Altered Arctic Climate Forcing, *Science*, **318**, 1381–1384.
- Melillo, J. M., D. W. Kicklighter, A. D. McGuire, W. T. Peterjohn, and K. M. Newkirk (1995), Global change and its effects on soil organic carbon stocks, in *Role of Nonliving Organic Matter in the Earth's Carbon Cycle*, edited by R. G. Zepp and C. H. Sontaff, pp. 175–189, John Wiley, New York.
- Myhre, C. L., et al. (2007), Regional aerosol optical properties and radiative impact of the extreme smoke event in the European Arctic in spring 2006, *Atmos. Chem. Phys.*, **7**, 5899–5915.
- O'Neill, N. T., T. F. Eck, B. N. Holben, A. Smirnov, O. Dubovik, and A. Royer (2001), Bimodal size distribution influences on the variation of Angstrom derivatives in spectral and optical depth space, *J. Geophys. Res.*, **106**(D9), 9787–9806.

- O'Neill, N. T., T. F. Eck, A. Smirnov, B. N. Holben, and S. Thulasiraman (2003), Spectral discrimination of coarse and fine mode optical depth, *J. Geophys. Res.*, **108**(D17), 4559, doi:10.1029/2002JD002975.
- Pfister, G. G., P. G. Hess, L. K. Emmons, P. J. Rasch, and F. M. Vitt (2008), Impact of the summer 2004 Alaska fires on top of the atmosphere clear-sky radiation fluxes, *J. Geophys. Res.*, **113**, D02204, doi:10.1029/2007JD008797.
- Reid, J. S., and P. V. Hobbs (1998), Physical and optical properties of young smoke from individual biomass fires in Brazil, *J. Geophys. Res.*, **103**(D24), 32,013–32,030.
- Reid, J. S., T. F. Eck, S. A. Christopher, P. V. Hobbs, and B. N. Holben (1999), Use of the Angstrom exponent to estimate the variability of optical and physical properties of aging smoke particles in Brazil, *J. Geophys. Res.*, **104**(D22), 27,473–27,489.
- Reid, J. S., R. Koppmann, T. Eck, and D. Eleuterio (2005a), A review of biomass burning emissions: Part II. Intensive physical properties of biomass burning particles, *Atmos. Chem. Phys.*, **5**, 799–825. (Available at <http://www.atmos-chem-phys.org/acp/5/799/>)
- Reid, J. S., T. F. Eck, S. A. Christopher, R. Koppmann, O. Dubovik, D. P. Eleuterio, B. N. Holben, E. A. Reid, and J. Zhang (2005b), A review of biomass burning emissions: Part III. Intensive optical properties of biomass burning particles, *Atmos. Chem. Phys.*, **5**, 827–849.
- Schafer, J. S., T. F. Eck, B. N. Holben, P. Artaxo, and A. F. Duarte (2008), Characterization of the optical properties of atmospheric aerosols in Amazonia from long-term AERONET monitoring (1993–1995 and 1999–2006), *J. Geophys. Res.*, **113**, D04204, doi:10.1029/2007JD009319.
- Schmid, B., J. Michalsky, R. Halthore, M. Beauharnois, L. Harrison, J. Livingston, P. Russell, B. Holben, T. Eck, and A. Smirnov (1999), Comparison of aerosol optical depth from four solar radiometers during the fall 1997 ARM intensive observation period, *Geophys. Res. Lett.*, **26**(17), 2725–2728.
- Shaw, G. E. (1982), Atmospheric turbidity in the polar-regions, *J. Appl. Meteorol.*, **21**(8), 1080–1108.
- Shaw, G. E. (1995), The arctic haze phenomenon, *Bull. Amer. Meteorol. Soc.*, **76**(12), 2403–2413.
- Smirnov, A., B. N. Holben, T. F. Eck, O. Dubovik, and I. Slutsker (2000), Cloud screening and quality control algorithms for the AERONET data base, *Remote Sens. Environ.*, **73**, 337–349.
- Soja, A. J., N. M. Tchekbakova, N. H. F. French, M. D. Flannigan, H. H. Shugart, B. J. Stocks, A. I. Sukhinin, E. I. Parfenova, F. S. Chapin III, and P. W. Stackhouse Jr. (2007), Climate-induced boreal forest change: Predictions versus current observations, *Global Planet. Change*, **56**, 274–296.
- Stohl, A. (2006), Characteristics of atmospheric transport into the Arctic troposphere, *J. Geophys. Res.*, **111**, D11306, doi:10.1029/2005JD006888.
- Stohl, A., et al. (2006), Pan-Arctic enhancements of light absorbing aerosol concentrations due to North American boreal forest fires during summer 2004, *J. Geophys. Res.*, **111**, D22214, doi:10.1029/2006JD007216.
- Stone, R. S., G. Anderson, E. Andrews, E. Dutton, E. Shettle, and A. Berk (2007), Incursions and radiative impact of Asian dust in northern Alaska, *Geophys. Res. Lett.*, **34**, L14815, doi:10.1029/2007GL029878.
- Stone, R. S., G. P. Anderson, E. P. Shettle, E. Andrews, K. Loukachine, E. G. Dutton, C. Schaaf, and M. O. Roman III (2008), Radiative impact of boreal smoke in the Arctic: Observed and modeled, *J. Geophys. Res.*, **113**, D14S16, doi:10.1029/2007JD009657.
- Turetsky, M., K. Wieder, L. Halsey, and D. Vitt (2002), Current disturbance and the diminishing peatland carbon sink, *Geophys. Res. Lett.*, **29**(11), 1526, doi:10.1029/2001GL014000.
- Turquetly, S., et al. (2007), Inventory of boreal fire emissions for North America in 2004: Importance of peat burning and pyroconvective injection, *J. Geophys. Res.*, **112**, D12S03, doi:10.1029/2006JD007281.
- Ward, D. E., W. M. Hao, R. A. Susott, R. E. Babbitt, R. W. Shea, J. B. Kaufman, and C. O. Justice (1996), Effect of fuel composition on combustion efficiency and emission factors for African savanna ecosystems, *J. Geophys. Res.*, **101**(D19), 23,569–23,576.
- Warneke, C., et al. (2009), Biomass burning in Siberia and Kazakhstan as an important source for haze over the Alaskan Arctic in April 2008, *Geophys. Res. Lett.*, **36**, L02813, doi:10.1029/2008GL036194.
- F. S. Chapin, Institute of Arctic Biology, University of Alaska, Fairbanks, AK 99775, USA.
- O. Dubovik, Laboratoire d'Optique Atmosphérique, CNRS Université de Lille, 1 Bat P5 Cite Scientifique, 59655 Villeneuve d'Ascq CEDEX, France.
- T. F. Eck, D. Giles, B. N. Holben, W. W. Newcomb, J. S. Schafer, A. Sinyuk, I. Slutsker, A. Smirnov, and M. Sorokine, NASA, GSFC, Code 614.4, Greenbelt, MD 20771, USA. (thomas.f.eck@nasa.gov)
- E. J. Hyer and J. S. Reid, Aerosol and Radiation Section, Marine Meteorology Division, Naval Research Laboratory, 7 Grace Hopper Avenue, Stop 2, Monterey, CA 93943-5502, USA.
- N. T. O'Neill, CARTEL, Dépt de géomatique appliquée, Université de Sherbrooke, Sherbrooke, QC J1K 2R1, Canada.
- G. E. Shaw, Geophysical Institute, University of Alaska, Fairbanks, AK 99775, USA.
- J. R. Vande Castle, Biology Department-MS03 2020, University of New Mexico, CERIA Building #83, Albuquerque, NM 87131-0001, USA.
- E. Vermote, Department of Geography, University of Maryland, College Park, MD 20742, USA.